Analysis of Aftercavity Interaction in European ITER Gyrotrons and in the Compact Sub-THz Gyrotron FU CW-CI

Olgierd Dumbrajs & Toshitaka Idehara

Journal of Infrared, Millimeter, and Terahertz Waves

ISSN 1866-6892
Volume 33
Number 12

J Infrared Milli Terahz Waves (2012)
33:1171-1181
DOI 10.1007/s10762-012-9934-6

Springer

J Infrared Milli Terahz Waves (2012) 33:1171–1181
DOI 10.1007/s10762-012-9934-6

Analysis of Aftercavity Interaction in European ITER Gyrotrons and in the Compact Sub-THz Gyrotron FU CW-CI

Olgierd Dumbrajs · Toshitaka Idehara

Received: 28 May 2012 / Accepted: 30 August 2012 /
Published online: 8 September 2012

Abstract Possibilities of arising of aftercavity interaction are analyzed in the ITER 170 GHz 2 MW coaxial cavity gyrotron and the 170 GHz 1 MW cylindrical cavity gyrotron, as well as in the compact 394.5 GHz low power gyrotron FU CW-CI. Also, the simulations for the gyrotron efficiency in the presence of aftercavity interaction are performed in the cold cavity approximation. Results of the analysis illustrate the subtle interplay between the geometry of the output taper and the profile of the magnetic field.

Keywords Gyrotron · ITER · DNP-NMR spectroscopy

1 Introduction

The essence of the so called aftercavity interaction (ACI) in gyrotrons is the possible fulfillment of the cyclotron resonance condition between electrons and the traveling wave in some cross-sections of the tapered magnetic field and waveguide radius

$$\omega - k_z v_z \approx s \cdot \Omega \tag{1}$$

Here $\omega=2\pi f$ is the wave frequency, k_z is the axial wavenumber, v_z is the axial electron velocity, s is the harmonic number, and Ω is the electron cyclotron frequency. The strength of ACI depends on the strength of the coupling of electrons to the RF field. This coupling depends on the ratio of the electron beam radius R_b to the waveguide wall radius R_w.

The name ACI was coined in [1] where it was found that in gyrotrons without energy recovery this interaction reduces the efficiency by 5-10 %, but in gyrotrons with energy

O. Dumbrajs (✉)
Institute of Solid State Physics, University of Latvia, Kengaraga Street 8, LV-1063 Riga, Latvia
e-mail: olgerts.dumbrajs@lu.lv

O. Dumbrajs · T. Idehara
Research Center for Development of Far-Infrared Region, University of Fukui (FIR FU), 3-9-1 Bunkyo, Fukui-shi 910-8507, Japan

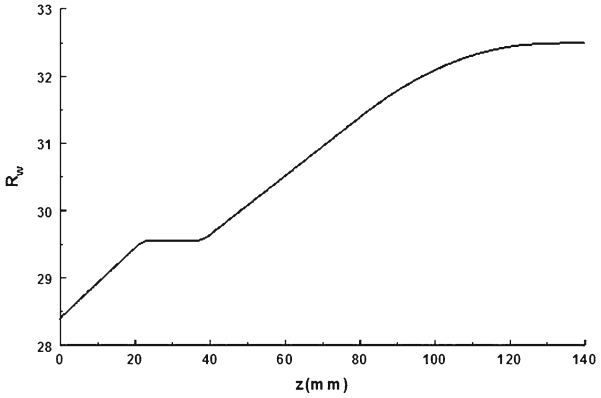

Fig. 1 Cavity wall radius as a function of longitudinal coordinate.

recovery the efficiency is reduced even by 20-30 %. This study was extended in [2] by analyzing the influence of the electron energy spread on ACI. In [3–5] the experimental observations of the effect of an ACI interaction in a single-stage depressed collector high-efficiency, 1.5 MW, 110 GHz gyrotron oscillator were presented. In experiments it was found that the observed efficiency of 50 % would have been about 60 % in the absence of the ACI. In [6] different ways to extend multimode simulations in the presence of ACI are discussed. In [7] the ACI in the quasi-optical launcher was analyzed and possible mitigation techniques were assessed. Simple analytic theory for finding conditions resulting in the reduction of the ACI effect was developed in [8] and [9]. In [10] the results of the efficiency study of a 670 GHz gyrotron operating at $TE_{31,8}$ mode with inclusion of ACI were presented. It was found that in this gyrotron the ACI causes only slight variations in the efficiency. The concept of the so called dynamic ACI oscillations was introduced in [11]. This type of ACI tries to explain arising of spurious parasitic oscillations observed in experiments as a result of interaction in the uptaper/launcher region of the tube. Such oscillations in the W7-X series gyrotron SN4R were examined in [12]. In the present paper we use the formalism developed in [8] to analyze the role of the ACI in European ITER gyrotrons and in the compact sub-THz gyrotron FU CW CI developed at the Research Center for Development of Far-Infrared Region, University of Fukui in Japan, for application to the 600*MHz* Dynamic Nuclear Polarization (DNP)-enhanced Nuclear Magnetic Resonance (NMR) spectroscopy.

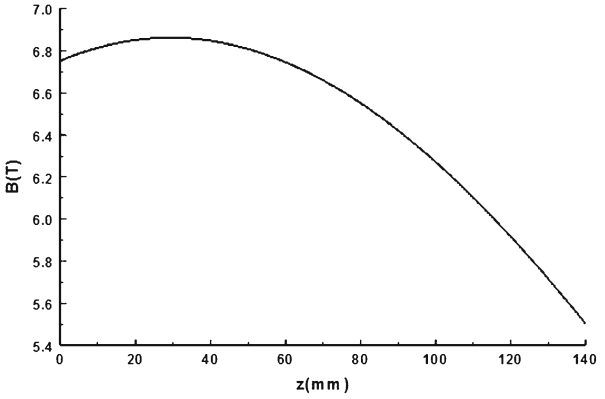

Fig. 2 Magnetic field as a function of longitudinal coordinate.

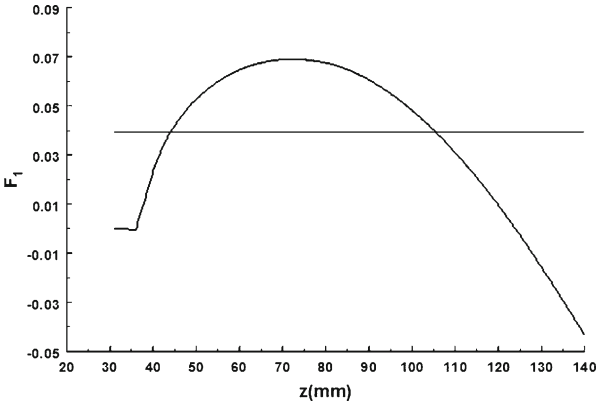

Fig. 3 The cyclotron resonance condition for ACI. The straight horizontal line shows the $1-\Omega_{middle}/\omega$ value.

2 Formalism

In Eq. (1) only the wave frequency ω remains constant along the z-axis. Both the Doppler term $k_z v_z$ and the electron cyclotron frequency Ω depend on the axial coordinate. From the dispersion relation

$$\omega^2 = \omega_{cut}^2 + c^2 k_z^2, \tag{2}$$

where $\omega_{cut} = \nu c/R_{wmiddle}$ and ν is the eigennumber, one can easily deduce the axial dependence of the axial wave number

$$k_z(z) = \frac{\omega}{c} \cdot \sqrt{1 - \frac{R_{wmiddle}^2}{R_w^2(z)}} \tag{3}$$

Here the subscript *middle* means the middle of the cavity. Of course, in real cavities excited near cutoff the axial wavenumber is not equal to zero, but has the finite length. However, when this length is much longer than a wavelength, the modes with one axial variation have $k_z << \omega/c$ and Eq. (3) is a good approximation [8] (there is a misprint in Eq. (3) of [8]).

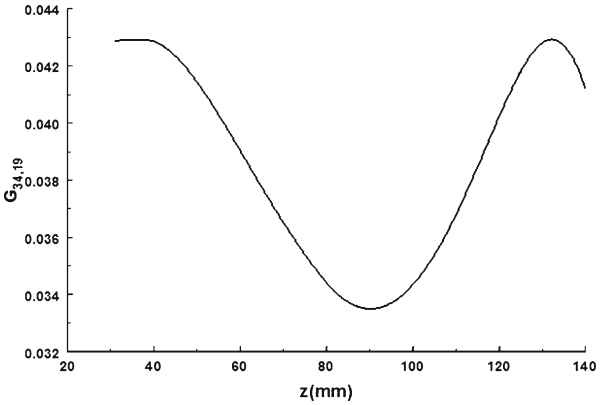

Fig. 4 The beam coupling as a function of longitudinal coordinate.

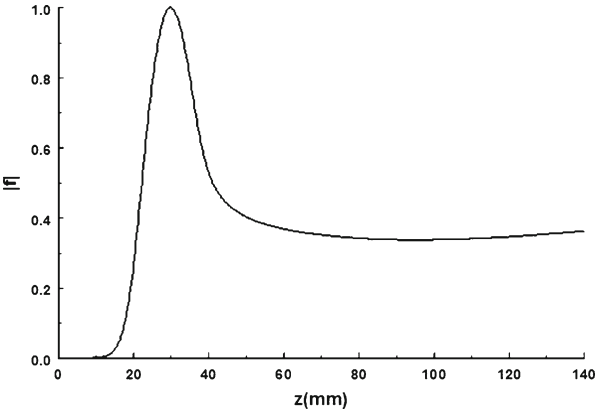

Fig. 5 RF field profile.

The standard equation

$$v_z(z) = \sqrt{v^2 - v_\perp^2(z)} \tag{4}$$

and the fact that in the absence of electromagnetic waves the axial dependence of the electron perpendicular velocity is given as

$$v_\perp(z) = v_{\perp middle}\sqrt{B(z)/B_{middle}} \tag{5}$$

where B is the magnetic field, gives us the axial dependence of the second multiplier in the Doppler term. Thus, the axial dependence of terms in Eq. (1) can be described by the following function:

$$F_1(z) = \sqrt{1 - \frac{R_{wmiddle}^2}{R_w^2(z)}} \cdot \beta_z(z) + \frac{B(z) - B_{middle}}{B_{middle}} \tag{6}$$

where $\beta_z = v_z/c$,

$$\beta_z(z) = \sqrt{1 - \frac{1}{\gamma^2} - \beta_{\perp middle}^2 \cdot \frac{B(z)}{B_{middle}}} \tag{7}$$

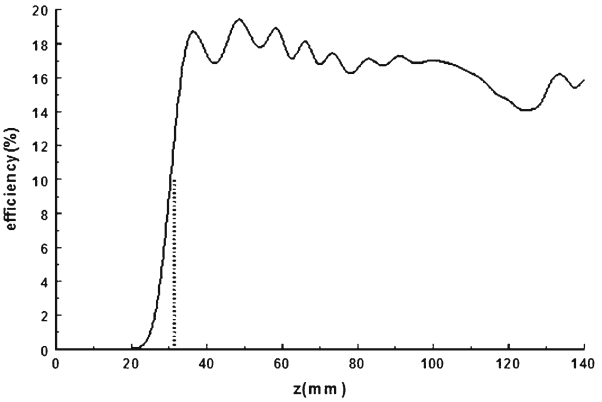

Fig. 6 Efficiency as a function of longitudinal coordinate. The vertical dashed line marks the middle of the cavity.

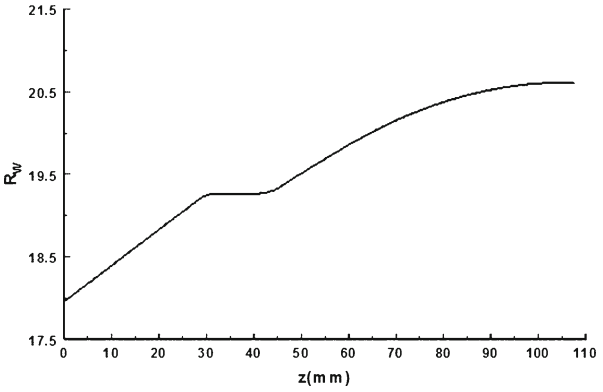

Fig. 7 Cavity radius as a function of longitudinal coordinate.

$$\gamma = 1 + \frac{U}{511} \tag{8}$$

$$\beta_{\perp middle} = \frac{\alpha}{\gamma} \cdot \sqrt{\frac{\gamma^2 - 1}{1 + \alpha^2}} \tag{9}$$

Here U is accelerating voltage in kV and α is the pitch factor. Correspondingly, the cyclotron resonance condition for the ACI can be given as

$$F_1 = 1 - s \cdot \Omega_{middle}/\omega \tag{10}$$

The coupling factor for a thin annular beam and a transverse-electric $TE_{m,p}$ wave in a cylindrical wave guide is given as

$$G_{m,p} = J^2_{m\pm s}\left(\nu_{m,p} R_b / R_w\right) \tag{11}$$

where J is the Bessel function, m and $\nu_{m,p}$ are the azimuthal index and the eigennumber of the mode respectively, and R_b is the electron beam radius. In a coaxial wave guide this coupling is given as [13]:

$$G_{m,p} = \left[J_{m\pm s}\left(\chi_{m,p} R_b / R_w\right) H_1 - N_{m\pm s}\left(\chi_{m,p} R_b / R_w\right) H_2\right]^2 \tag{12}$$

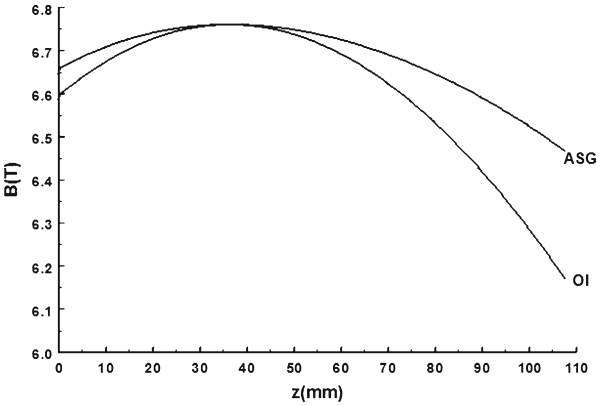

Fig. 8 Profiles of magnetic fields. OI means Oxford instruments and ASG means Ansaldo (Italian company).

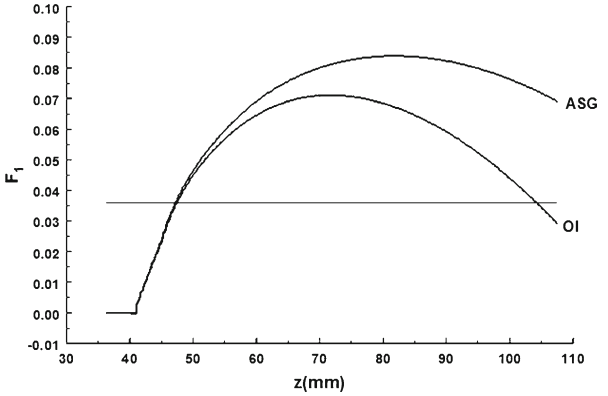

Fig. 9 The cyclotron resonance condition for ACI. The straight horizontal line shows the $1-\Omega_{middle}/\omega$ value.

Here N is the Neumann function and

$$H_1 = N'\left(\frac{\chi_{m,p}}{C}\right) + W \cdot N\left(\frac{\chi_{m,p}}{C}\right) \tag{13}$$

$$H_2 = J'\left(\frac{\chi_{m,p}}{C}\right) + W \cdot J\left(\frac{\chi_{m,p}}{C}\right) \tag{14}$$

$$C = R_w/R_{in} \tag{15}$$

where R_{in} is the radius of the insert with longitudinal corrugations, and

$$W = \frac{l}{q}\tan\left(\frac{2\pi}{\lambda}d\right) \tag{16}$$

where l is the width of the grooves, q is the period of the corrugations, d is the depth of the grooves, and λ is the wavelength. According to the Busch theorem the axial dependence of the electron beam radius can be given as

$$R_b(z) = R_{b\,middle}\sqrt{B_{middle}/B(z)} \tag{17}$$

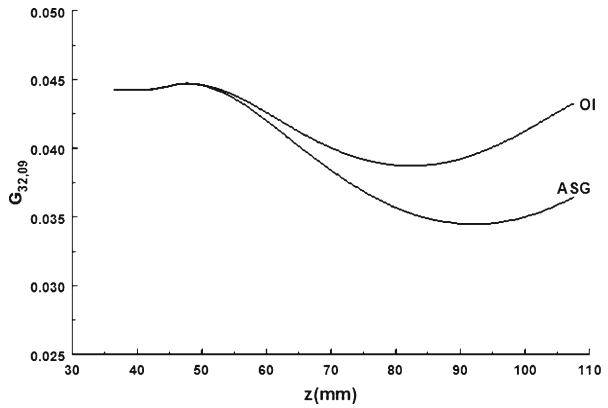

Fig. 10 The beam coupling for the two magnetic field profiles.

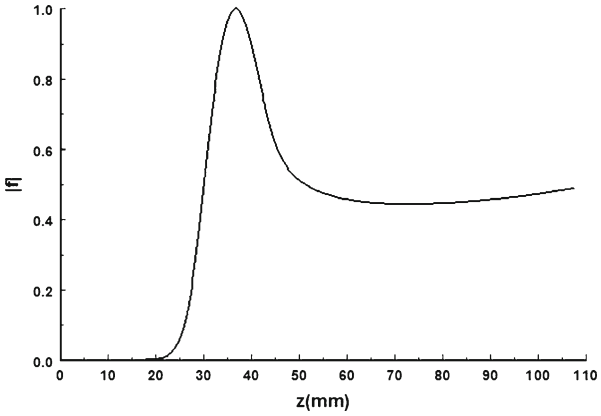

Fig. 11 RF field profile.

which leads to the axial dependence of the couplings (11) and (12). It should be noted that in the case of a coaxial waveguide the eigenvalue $\chi_{m,p}$ and the ratio (15) also depend on the axial coordinate z.

3 Coaxial Cavity Gyrotron

The operating mode of the $170\,GHz$ $2\,MW$ coaxial cavity gyrotron [14] is $TE^{-}_{34,19}$ and the operating parameters are:R_b=10.0mm, B_{middle}=6.86T, current 80A, voltage 90kV, and pitch factor 1.3. The wall radius is shown in Fig. 1 and the profile of the magnetic field in Fig. 2.

The cyclotron resonance condition for ACI is shown in Fig. 3.

It can be seen that the resonance condition is fulfilled at the beginning of the output taper at z=43mm and deep into the output taper at z=106mm. The beam coupling is shown in Fig. 4. It is evident that, as expected, the coupling is large at the first resonance point. However, at the second resonance point it also remains relatively large (is smaller by factor 1.26). Thus, for the operating voltage and pitch factor some ACI is expected in the coaxial gyrotron. To verify this conclusion we performed cold cavity calculations. In Fig. 5 we show RF field profile in the cavity and in Fig. 6 the efficiency as a function of the longitudinal coordinate.

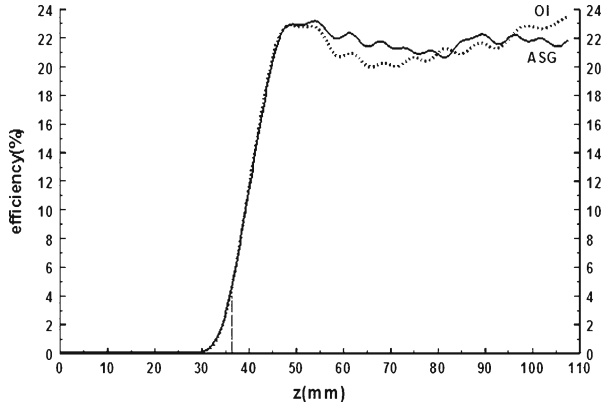

Fig. 12 Efficiency as a function of longitudinal coordinate . The vertical dashed line marks the middle of the cavity.

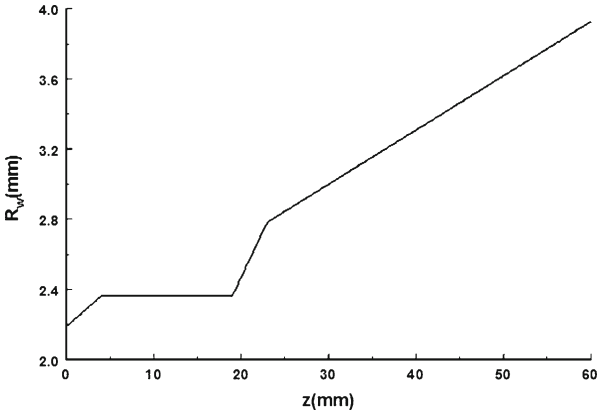

Fig. 13 Cavity radius as a function of longitudinal coordinate.

It can be seen that the interaction begins at around $z=20\,mm$, i.e. at the beginning of the straight section (Fig. 1). As expected, efficiency reaches its maximum value at the beginning of the output taper, where the first resonance condition is fulfilled. It is interesting that interaction in the output reduces the efficiency. Thus, in this case ACI plays a negative role. To avoid this effect one should modify either the geometry of the output taper, or the profile of the magnetic field, in order to destroy the second resonance.

4 Cylindrical Cavity Gyrotron

The operating mode of the $170\,GHz$ $1\,MW$ cylindrical cavity gyrotron is $TE^{-}_{32,09}$. This gyrotron is under development in Europe as a fall back solution for the case if the coaxial gyrotron program fails. The operating parameters of the gyrotron are: $R_b=9.50\,mm$, $B_{middle}=6.76\,T$, current $45A$, voltage $79\,kV$, and pitch factor 1.3. The wall radius is shown in Fig. 7 and the profiles of two different magnetic fields are shown in Fig. 8.

The cyclotron resonance conditions for ACI is shown in Fig. 9 and the beam couplings in Fig. 10.

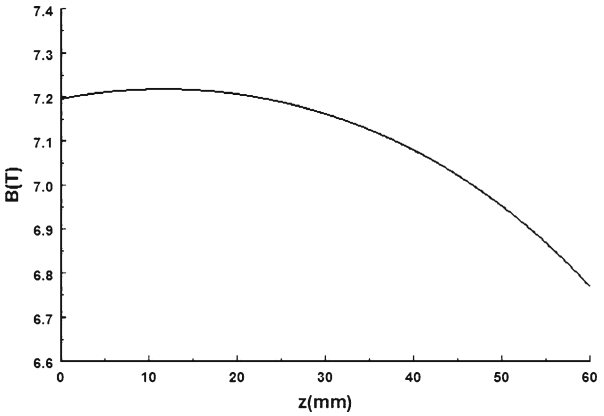

Fig. 14 Magnetic field profile.

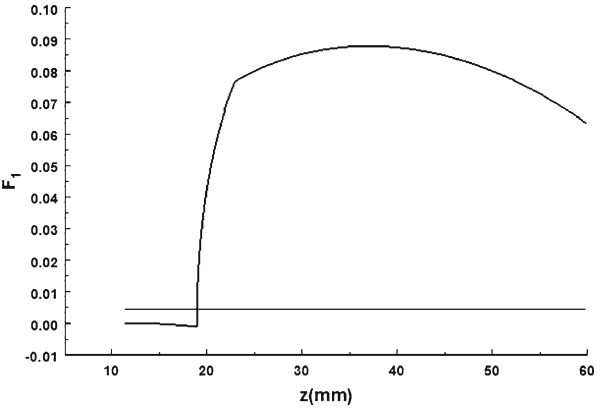

Fig. 15 The cyclotron resonance condition for ACI. The straight horizontal line shows the $1-2\cdot\Omega_{middle}/\omega$ value.

It can be seen that for the two magnetic field profiles the resonance condition is fulfilled properly at the beginning of the output taper at $z=47\,mm$. For the OI magnetic field profile the second resonance condition occurs deep into output taper at $z=105\,mm$ but for the ASG magnetic field profile there is no second resonance point. The corresponding beam couplings are shown in Fig. 10. ACI can be expected in the case of OI magnet. Calculations confirm this. The RF field profile is shown in Fig. 11 and efficiencies in Fig. 12.

Indeed, as can be seen, in the case of the OI magnet the efficiency varies in the output taper due to ACI noticeably. First it plays a negative role reducing efficiency from 24 % to 20 % at $z=65\,mm$ and then a positive role increasing efficiency to 24 % at the end of the output taper. Thus, it would be unpleasant to have the output taper as short as $65\,mm$. In the case of the ASG magnet there is no ACI and the efficiency remains practically constant in the output taper.

5 Compact Sub-THz Gyrotron FU CW-CI

The operating mode is $TE^{+}_{2,6}$ at the second harmonic ($s=2$). The operating parameters are: $R_b=0.63\,mm$, $B_{middle}=7.19\,T$, current $0.2\,A$, voltage $15\,kV$, and pitch factor 1.61. The wall radius is shown in Fig. 13 and the magnetic field profile in Fig. 14.

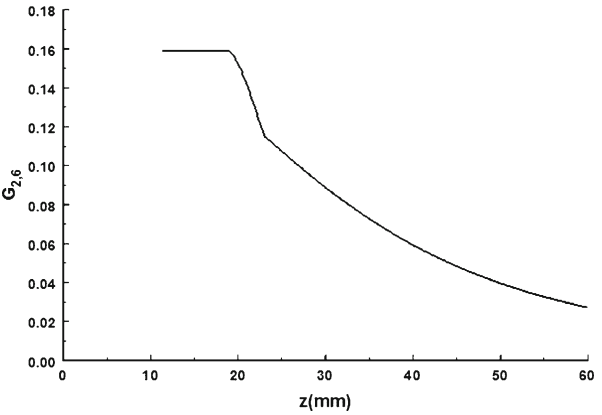

Fig. 16 The beam coupling.

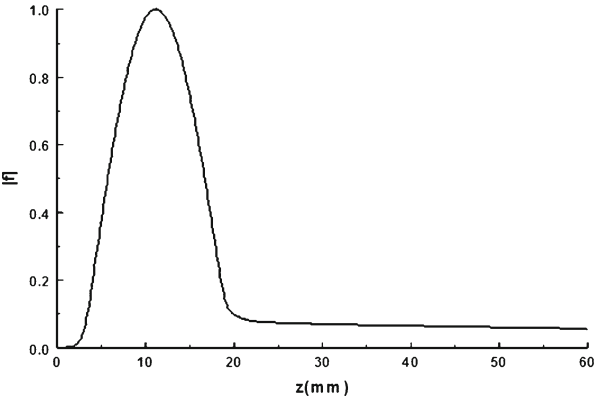

Fig. 17 RF field profile.

The cyclotron resonance condition for ACI is shown in Fig. 15, the beam coupling in Fig. 16, and RF field profile in the cavity in Fig. 17.

Since there is no resonance condition in the output taper and the coupling there is very weak, no ACI is expected in this gyrotron. Efficiency calculations confirm this, as can be seen in Fig. 18. It is interesting that in the experiment [15] a very low efficiency (0.4 %) has been measured in contrast to theoretical predictions (1.1 %). Since the present calculations do not find any ACI in this gyrotron, which in principle could be responsible for this discrepancy, other reasons should be considered. Most probably, in the experiment the value of the pitch factor was not 1.61 as assumed, but much lower: on the order of 1.20.

6 Conclusions

ACI can have a noticeable influence, both positive and negative, on the efficiency of the tube. Subtle interplay between the geometry of the output taper and the magnetic field profile should be analyzed in detail for each chosen set of gyrotron operating parameters best of all self-consistently. Since it is much easier (cheaper) to modify the geometry of the output taper than the profile of the given magnetic field, in specific designs one should first choose (fix) the geometry of the magnetic field and then optimize the geometry of the output taper, in order to achieve the highest possible efficiency for the desired operating parameters of the gyrotron.

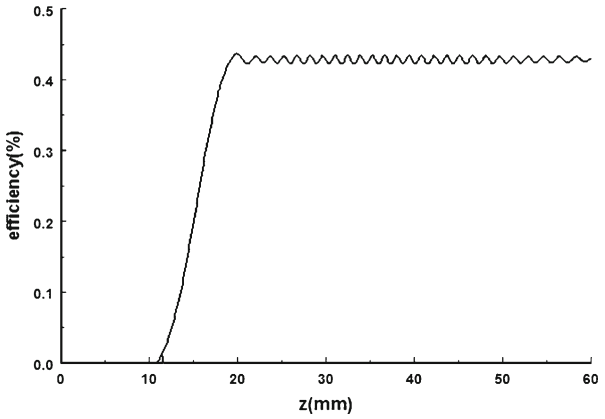

Fig. 18 Efficiency as a function of longitudinal coordinate. The middle of the cavity is at z= 11.5 mm. Here α=1.2 was used.

References

1. V.E. Zapevalov and M.A. Moiseev, Radiophys. Quantum Electron. **47**, 520 (2004).
2. N.A. Zavolsky, V.E. Zapevalov, and M.A. Moiseev, Radiophys. Quantum Electron. **49**, 108 (2006).
3. E.M. Choi, M.A. Shapiro, J.R. Sirigiri, and R.J. Temkin, Phys. Plasmas **14**, 093302 (2007).
4. Y. Hidaka, E.M. Choi, M.A. Shapiro, J.R. Sirigiri, and R.J. Temkin, Conference Proceedings, IVEC 2008, IEEE International Conference on Vacuum Electronics, Monterey, California, USA, April 22-24, 2008.
5. Y. Hidaka, E.M. Choi, I. Mastovsky, M.A. Shapiro, J.R. Sirigiri, and R.J. Temkin, Conference Proceedings, 33rd International Conference on Infrared Millimeter THz Waves, Pasadena, California, USA, September 15-19, 2008.
6. S. Kern and E. Borie, Conference Proceedings, 33rd International Conference on Infrared Millimeter THz Waves, Pasadena, California, USA, September 15-19, 2008.
7. S.R. Cauffman, Conference Proceedings, 33rd International Conference on Infrared Millimeter THz Waves, Pasadena, California, USA, September 15-19, 2008.
8. O.V. Sinitsyn and G.S. Nusinovich, Phys. Plasmas **16**, 023101 (2009).
9. O.V. Sinitsyn, G.S. Nusinovich, and T.M. Antonsen, Jr., Phys. Plasmas **17**, 083106 (2010).
10. R. Pu, G.S. Nusinovich, O.V. Sinitsyn, and T.M. Antonsen, Jr., Phys. Plasmas **18**, 023107 (2011).
11. S. Kern, K.A. Avramides, A.R. Choudhury, O. Dumbrajs, G. Gantenbein, S. Illy, A. Samartsev, A. Schlaich and M. Thumm, Conference Proceedings, 35th International Conference on Infrared Millimeter THz Waves, Rome, Italy, September 5-10, 2010.
12. A. Schlaich, A.R. Choudhury, G. Gantenbein, S. Illy, S. Kern, C. Lievin, A Samartsev and M. Thumm, Conference Proceedings, 36th International Conference on Infrared Millimeter THz Waves, Houston, Texas, USA, October 2-7, 2011.
13. O. Dumbrajs, M.Yu. Glyavin, V.E. Zapevalov, and N.A. Zavolsky, IEEE Trans. Plasma Sci. **28**, 588 (2000).
14. G. Gantenbein, T. Rzesnicki, B. Piosczyk, S. Kern, S. Illy, J. Jin, A. Samartsev, A. Schlaich, and M. Thumm, 23rd IAEA Fusion Energy Conference, Daejon, Korea, 11-16 October 2010, ITR/2-5Rc, p. 517.
15. T. Idehara, J.C. Mudiganti, La Agusu, T. Kanemaki, I. Ogawa, T. Fujiwara, Y. Matsui, and K. Ueda, J. Infrared Millimeter and Terahertz Waves **13**, 724 (2012).